Chinese Journal of Catalysis 37 (2016) 1381–1388

available at www.sciencedirect.com

ScienceDirect

journal homepage: www.elsevier.com/locate/chnjc

Article

Hydrothermal synthesis of nanosized ZSM-22 and their use in the catalytic conversion of methanol

Lei Chen [a,b], Peng Lu [a,b], Yangyang Yuan [a], Li Xu [a], Xiaomin Zhang [a,*], Lei Xu [a,#]

[a] *Dalian National Laboratory for Clean Energy, Dalian Institute of Chemical Physics, Chinese Academy of Sciences, Dalian 116023, Liaoning, China*
[b] *University of Chinese Academy of Sciences, Beijing 100049, China*

ARTICLE INFO

Article history:
Received 29 January 2016
Accepted 15 March 2016
Published 5 August 2016

Keywords:
Nanosized ZSM-22 zeolite
Hydrothermal synthesis
Conversion of methanol

ABSTRACT

ZSM-22 zeolite with different crystal lengths was prepared using a modified hydrothermal method. Rotation speed, Si/Al molar ratio and co-solvent have important effects on the crystal size of ZSM-22. The nanosized zeolite samples were characterized by X-ray diffraction, X-ray fluorescence, nitrogen adsorption, scanning electron microscopy, temperature-programmed desorption of ammonia and solid state nuclear magnetic resonance. The catalytic performance of nanosized ZSM-22 was tested using the conversion of methanol. Compared to conventional ZSM-22, the nanosized ZSM-22 zeolite exhibited superior selectivity to ethylene and aromatics and lower selectivity to propylene. Stability against deactivation was clearly shown by the nanosized ZSM-22 zeolite. A higher external surface area and smaller particle size make this nanosized ZSM-22 zeolite attractive for catalytic applications.

1. Introduction

Due to their diversity of structures and unique properties, zeolites are widely used in a variety of applications including catalysis, sorption-separation and ion exchange processes. The synthesis and application of zeolites have attracted a great deal of interest [1–4]. The excellent performance in a variety of areas by zeolites depends on their structural properties such as crystal size and chemical composition [5–11]. In order to optimize zeolite performance, the synthesis of zeolite with a novel structure has gained much attention in the past decades.

Lately, the preparation and application of nanosized zeolites have attracted considerable attention. Compared to conventional molecular sieves of micron size, a zeolite with a crystal size in the nano-scale produced significant benefits in performance in separation and catalysis [5,12–16]. The nanosized zeolites have a large external surface and high surface activity. So it is preferred where the desired catalytic reactions take place on or near the external surface of the crystal like hydroisomerization of long chain paraffins [17,18]. In addition, compared to the conventional micrometer-sized zeolites, smaller zeolite crystals have short diffusion path lengths. Therefore, it is favorable to use a nanosized zeolite in some reactions because mass transfer limitation is avoided. Furthermore, it has been shown that deactivation can be slowed down on smaller crystals due to their larger specific external area. Currently, many strategies have been developed to prepare nanosized zeolite crystals. The most common method uses a clear precursor solution with an excess of the organic template [14]. With the development of the synthesis technology of nanomaterials, some new strategies such as confined-space synthesis [15,16], seed-assisted approach [19], ionothermal synthesis,

* Corresponding author. Tel: +86-411-84379500; E-mail: zhangxm@dicp.ac.cn
# Corresponding author. Tel/Fax: +86-411-82463032; E-mail: leixu@dicp.ac.cn
This work was supported by the National Natural Science Foundation of China (21506202).
DOI: 10.1016/S1872-2067(15)61099-3 | http://www.sciencedirect.com/science/journal/18722067 | Chin. J. Catal., Vol. 37, No. 8, August 2016

microwave and sonication synthesis approaches [20] as well as microreactor synthesis [21] have appeared. Up to now, different zeolite structures on the nano-scale have been prepared and well studied including the FAU, MFI, MEL, SOD, GIS, LTA, BEA, AEI and CHA framework types [11,13,22–25]. In short, nanosized zeolites are ready to play an important role in a variety of application areas, and new fields will also open up due to their exceptional properties. So broadening the kind of nanosized zeolites and the development of mild synthesis methods is of great importance.

ZSM-22 with a TON topology structure was first synthesized by Dwyer et al. [26]. It features 1-dimensional 10-membered ring channels and tear-drop-shaped pores with a diameter of 0.45 nm × 0.55 nm. ZSM-22 exhibits excellent catalytic activity and shape selectivity for the hydroisomerization of long chain *n*-paraffins [27], skeletal isomerization of *n*-butene [28] and toluene alkylation [29]. Due to its potential application in industry, more interests have been focused on the synthesis of ZSM-22. Hydrothermal synthesis is the most commonly method to prepare ZSM-22. The crystal sizes of ZSM-22 are usually in the range of 2–15 μm [30–34]. It has been reported that the synthesis of ZSM-22 is usually carried out under vigorous stirring conditions (usually up to 400 r/min is recommended) in order to prevent co-crystallization of ZSM-5 and cristobalite. Because of the metastable structure of ZSM-22, one of the biggest challenges in ZSM-22 synthesis is the narrow synthesis range. Babav et al. [31] have reported hydrothermal synthesis of pure ZSM-22 under mild conditions using an autoclave, in which the synthesis vessel was rotated horizontally. However, the particle size of the obtained ZSM-22 was about 1 μm, which was still too large for use as an effective catalyst. Muraza et al. [34] used a microwave-assisted hydrothermal synthesis method to prepare submicrometer ZSM-22 zeolite. The crystal size of the obtained ZSM-22 was in the range of 400–500 nm. However, the crystal size was not adjustable and the synthesis process needed a high power microwave reactor. Therefore, it still remains a great challenge to synthesis pure nanosized ZSM-22 under mild hydrothermal synthesis conditions.

Here, we report the synthesis of pure nanosized ZSM-22 crystals using a modified hydrothermal method. The influences of the rotation speed, Si/Al molar ratio and ethanol as co-solvent on the crystal size were studied. The performance of the nanosized and conventional ZSM-22 was investigated in the conversion of methanol.

2. Experimental

2.1. Preparation of ZSM-22

Nanosized ZSM-22 was synthesized by a modified traditional hydrothermal method. 1,6-Diaminohexane (DAH) was used as the structure directing agent, and silica sol and aluminum sulfate were used as silicon source and aluminum source, respectively. A typical hydrothermal synthesis procedure of the pure nanosized ZSM-22 zeolite was carried out as follows. In a Teflon beaker, a clear solution was prepared by mixing KOH, $Al_2(SO_4)_3{\cdot}18H_2O$ and deionized water under stirring by a magnetic stirrer. Then DAH was dissolved in deionized water and added into the Teflon beaker under stirring, followed by stirring for 1 h. Silica sol (30% SiO_2) was added to the obtained clear solution under stirring. The resulting gel, having a molar composition of $x SiO_2{:}Al_2O_3{:}9KOH{:}27DAH{:}3600H_2O$ was stirred for another 2 h to get the final gel, where x was in the range of 30–90. Then the Teflon-lined vessel was sealed in a stainless container and aged for 6 h at 298 K. Finally, the gel was stirred at varying rotation speed (0, 10, 20, 40 and 50 r/min) in a rotary furnace at 433 K for 38 h. After crystallization, the autoclave was quenched in cold water and white crystals were recovered by filtrating and washing with deionized distilled water. The obtained samples were dried at 353 K overnight. The samples then were calcined at 823 K for 24 h to remove the template. The obtained samples were denoted as N-ZSM-22.

Microsized ZSM-22 was synthesized by a similar method except that ethanol was added as co-solvent when dissolving KOH and $Al_2(SO_4)_3{\cdot}18H_2O$. The obtained samples were denoted as M-ZSM-22.

The calcined zeolites (K-N-ZSM-22 and K-M-ZSM-22) were ion exchanged with 1 mol/L NH_4Cl three times and calcined again to obtain H-N-ZSM-22 and H-M-ZSM-22.

2.2. Characterization of ZSM-22

X-ray diffraction (XRD) patterns were recorded by a PANalytical X'Pert Pro X-ray diffractometer using Cu K_α radiation (λ = 1.5418 Å) at 40 kV and 40 mA. The 2θ angles were scanned from 5° to 65°. The particle size and morphology were measured by field emission scanning electron microscopy (FE-SEM, Hitachi, SU8020). The chemical composition was determined by a Philips Magix-601 X-ray fluorescence spectrometer (XRF). N_2 adsorption isotherms were measured on a Micromeritics ASAP 2020 system at 77 K. The total surface area was calculated based on the Brunauer-Emmett-Teller (BET) equation. The micropore volume and micropore surface area were evaluated by the *t*-plot method. The mesopore volume was calculated by the BJH method.

All the solid state nuclear magnetic resonance (NMR) experiments were performed on a Bruker AvanceIII 600 spectrometer equipped with a 14.1 T wide bore magnet. The resonance frequencies were 156.4 and 119.2 MHz for ^{27}Al and ^{29}Si, respectively.

The acidity of H-ZSM-22 was determined by temperature-programmed desorption of ammonia (NH_3-TPD) on a chemical adsorption instrument (Micromeritics AutoChem 2920). A 0.20 g sample was loaded in a U-shaped reactor and pretreated at 923 K for 30 min under He atmosphere. After cooling to 373 K, the sample was saturated with NH_3, followed by purging with He to remove physisorbed ammonia. Ammonia desorption was carried out in a He flow (40 mL/min) by increasing the temperature from 373 to 873 K with a heating rate of 10 K/min and monitored by a thermal conductivity detector (TCD).

2.3. Catalytic tests and product analysis

The ZSM-22 sample was pressed and sieved to 20–40 mesh

and then loaded using 1 g of sample into a fixed-bed reactor with an inner diameter of 10 mm and a bed height of 40 mm. The temperature of the fixed-bed reactor was increased from 298 to 823 K with a heating rate of 15 K/min and then kept at 823 K for 60 min to activate the catalyst. After the catalyst was activated, the temperature was then cooled to the reaction temperature.

Methanol was fed into the reactor by a high performance liquid chromatography infusion pump and vaporized. Then by passing a carrier gas (He), methanol vapor was fed into the catalyst bed and reacted under the catalysis of the catalyst. The product was kept at 493 K and analyzed by gas chromatography (GC) online on an Agilent 7890A system with an FID detector equipped with a CP WAX capillary column and a TCD detector equipped with a PLOT Q capillary column. The conversion and selectivity were calculated on a CH_2 basis. Dimethyl ether (DME) was considered as reactant in the calculation. Methanol conversion (X) and product selectivity (S) were calculated by the following equations:

$$X = (n_{(\text{fed of MeOH})} - n_{(\text{unreacted MeOH})})/n_{(\text{fed of MeOH})} \times 100\%$$

$$S = n_{(\text{carbon atom in a product})}/(n_{(\text{fed of MeOH})} - n_{(\text{unreacted MeOH})}) \times 100\%$$

3. Results and discussion

3.1. Synthesis of nanosized ZSM-22 zeolite

3.1.1. Effect of rotation speed

It is important to synthesize a pure zeolite for many applications. ZSM-22 has a metastable crystal structure, and the synthesis conditions are harsh. It has been reported that high speed (usually up to 400 r/min) mixing of the synthesis gel during the hydrothermal synthesis process is required in order to prevent generating impurities of ZSM-5 and cristobalite [31]. It still remains a great challenge to synthesize pure ZSM-22, not to mention nanosized ZSM-22.

First of all, N-ZSM-22 with a Si/Al molar ratio of 60 was synthesized under different rotation speeds. The XRD patterns of the samples are shown in Fig. 1. It was found that an amorphous phase was formed under static synthesis conditions similar to the findings of others. During the synthesis of N-ZSM-22 in the rotating oven under varying rotation speed, the XRD patterns of the product showed diffraction peaks characteristic of ZSM-22 zeolite with the TON topology. No other peak was observed suggesting pure N-ZSM-22. It has been reported that the synthesis of pure ZSM-22 depends mostly on the homogeneous mixing of the synthesis gel during the hydrothermal synthesis process. Thus, this result suggested that the present preparation method in a rotating oven at a relatively slow rotation speed could effectively mix the synthesis gel homogeneously and give phase-pure ZSM-22.

In order to investigate the morphology and crystal size of the obtained ZSM-22, SEM was used to characterize the zeolite. As displayed in Fig. 2, N-ZSM-22 possessed a uniform needle-like morphology, typical of ZSM-22, with a particle length ranging from 150 to 250 nm. These N-ZSM-22 particles were much shorter than those previously reported, which were synthesized under more severe conditions. The crystallization of a zeolite includes two parts: the formation of a crystal nucleus and growth of the crystal nucleus. In order to obtain a pure zeolite, a certain rotation speed was needed to ensure the homogenous mixing of the synthesis gel and to promote the formation of crystal nucleus. However, the growth space will be restricted because of the aggregation of crystal nucleus, thus limiting the size of the resulting crystal grain. When the rotation speed is slow during the growth process, the crystal nuclei of N-ZSM-22 do not aggregate very well, so the resulting crystal size of N-ZSM-22 is larger. When the rotation speed is faster, the crystal nuclei of N-ZSM-22 aggregated more, limiting the growth space of the crystal nucleus. However, the originally formed crystal nucleus aggregation is broken due to the larger external forces, and this resulted in the secondary growth of the crystal particle during the process of crystal nucleus growth; hence, the particle size is larger. That is to say, in order to get a smaller particle size, a moderate rotation speed by the present synthesis method was needed.

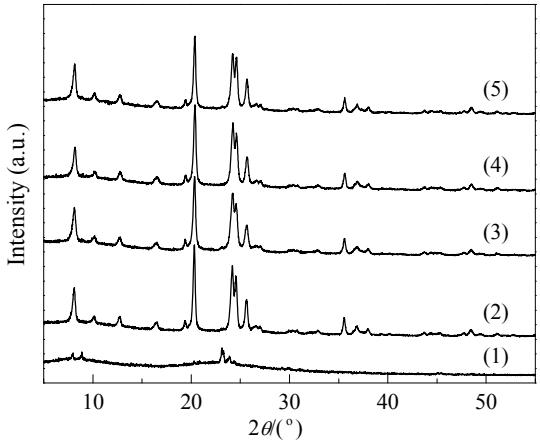

Fig. 1. XRD patterns of N-ZSM-22 with Si/Al ratio of 60 synthesized under varying rotation speeds (r/min): (1) 0; (2) 10; (3) 20; (4) 40; (5) 50.

3.1.2. Effect of Si/Al ratio

A series of nanosized zeolite with varying Si/Al ratios were also prepared under the rotation speed of 20 r/min. The effect

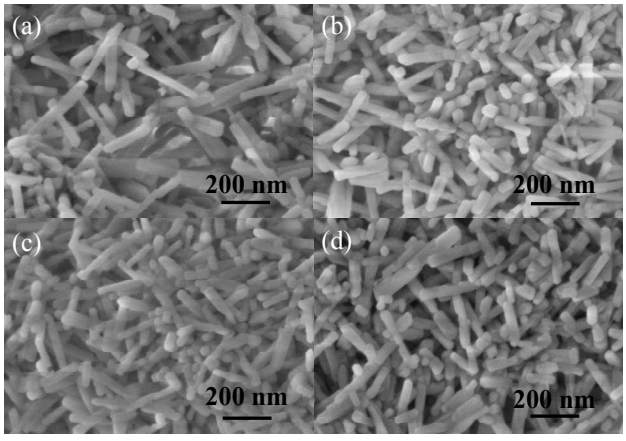

Fig. 2. SEM images of N-ZSM-22 with Si/Al ratio of 60 synthesized under varying rotation speeds (r/min): (a) 10; (b) 20; (c) 40; (d) 50.

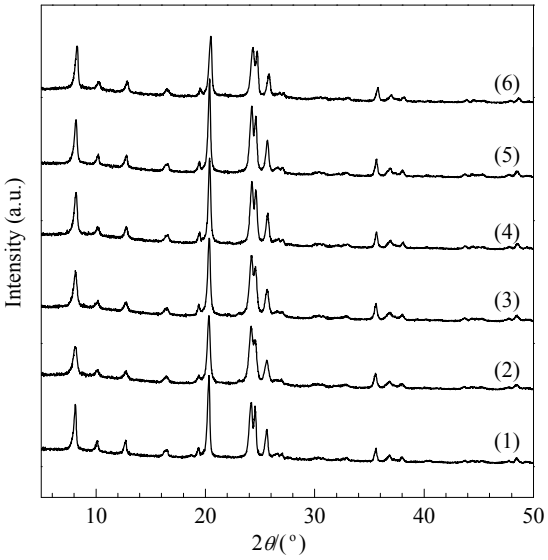

Fig. 3. XRD patterns of N-ZSM-22 with varying Si/Al ratios: (1) 30; (2) 45; (3) 60; (4) 75; (5) 90. (6) M-ZSM-22 with Si/Al ratio of 90.

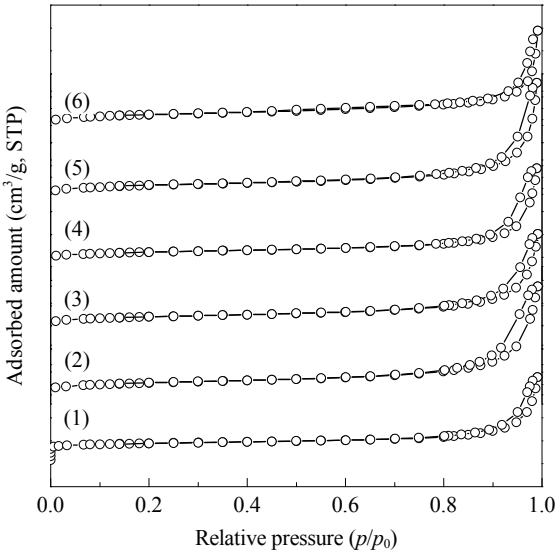

Fig. 5. N_2 adsorption isotherms of N-ZSM-22 with varying Si/Al ratios: (1) 30; (2) 45; (3) 60; (4) 75; (5) 90. (6) M-ZSM-22 with Si/Al ratio of 90.

of Si/Al ratio on the crystal size of nanosized ZSM-22 was investigated. N-ZSM-22 was synthesized at a molar ratio of xSiO$_2$:Al$_2$O$_3$:9KOH:27DAH:3600H$_2$O at 433 K for 38 h, where x was varied from 30 to 90. The resulting XRD patterns are shown in Fig. 3. As shown, no other peak was observed for the N-ZSM-22 samples with the Si/Al ratio from 30 to 90, indicating a high purity of the products.

The SEM images of N-ZSM-22 with different Si/Al ratios are shown in Fig. 4. It has been reported for ZSM-22 that the typical morphology of TON-type zeolite was needle-like crystallites with a length of about 2–15 μm [26,27,30,31,33,34]. According to the SEM images, all of the N-ZSM-22 crystals exhibited a needle-like morphology, and the crystal length of individual needles varied from 150 to 800 nm. The crystal length of N-ZSM-22 decreased from 800 to 150 nm with the increase of the Si/Al ratio from 30 to 60. Conversely, the crystal length increased from 150 to 650 nm when the Si/Al ratio continued to increase to 90. It has been reported that the Si/Al ratio affected the crystal size and morphology of ZSM-5 and ZSM-23 [35,36]. Shirazi et al. [35] found that by increasing the aluminum content of ZSM-5, the surface areas increased and the crystal size decreased. Liu et al. [36] found that the Si/Al ratio affected the ZSM-23 morphology. In this study, it was clear that the Si/Al ratio had a large effect on the crystal size of ZSM-22.

N_2 adsorption isotherms were used to estimate the porosity of the samples. Typical isotherms with a sharp uptake at a relative pressure p/p_0 above 0.01 are shown in Fig. 5. This indicated a characteristic micropore framework of N-ZSM-22. The detailed textural properties of the samples are listed in Table 1. Combined with the results above, some trends were observed for the data in Table 1. The external surface areas increased gradually with decreasing crystal size, which is in accordance with the reported results. The Si/Al ratio obtained from the XRF method was lower than in the original precursor gel, suggesting that part of the Si atoms were not incorporated into the

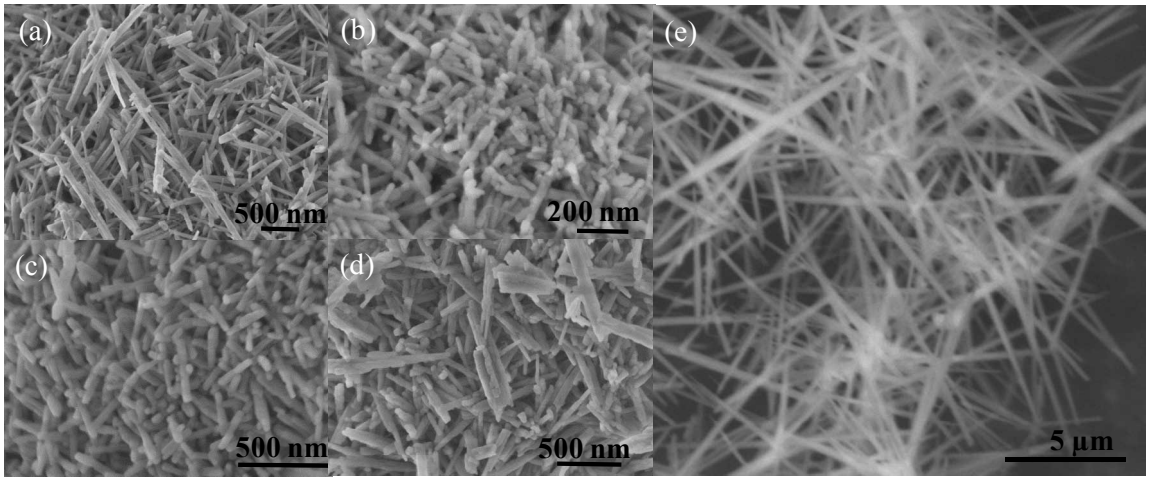

Fig. 4. SEM images of N-ZSM-22 with varying Si/Al ratios: (a) 30; (b) 45; (c) 75; (d) 90. (e) M-ZSM-22 with starting Si/Al ratio of 90.

Table 1
Surface area, pore volume and XRF results of ZSM-22 with different Si/Al ratios.

Sample	Original Si/Al ratio	Surface area (m^2/g)			Crystal size (μm)	Pore volume (cm^3/g)			Si/Al ratio by XRF
		BET [a]	Micropore [b]	External		Total [c]	Micropore [b]	Mesopore	
N-ZSM-22	30	150.6	104.4	46.3	0.80	0.17	0.05	0.12	30.8
N-ZSM-22	45	183.4	94.9	88.5	0.20	0.33	0.04	0.29	39.7
N-ZSM-22	60	235.1	165.0	70.1	0.15	0.25	0.08	0.17	51.3
N-ZSM-22	75	206.3	145.9	60.4	0.20	0.26	0.07	0.19	55.9
N-ZSM-22	90	209.7	158.4	51.3	0.65	0.21	0.07	0.14	66.9
M-ZSM-22	90	184.6	145.3	39.3	7.20	0.14	0.07	0.07	74.2

[a] BET method. [b] *t*-plot method. [c] Volume adsorbed at $p/p_0 = 0.99$.

framework of the zeolite. To confirm the coordination environment of the Al and Si atoms on a molecular level, ^{27}Al MAS NMR and ^{29}Si MAS NMR were performed for all the N-ZSM-22 samples. The spectra are shown in Fig. 6. In the ^{27}Al MAS NMR spectra of N-ZSM-22, two signals at δ = 55 and 0 were observed, which were assigned to framework Al species in the tetrahedral coordination state and extra-framework octahedral Al species, respectively. The intensity of the signal at δ = 0 decreased gradually with increasing Si/Al ratios. This result suggested that the amount of extra-framework octahedral Al species decreased with increasing Si/Al ratio. The signals with chemical shifts at δ = –112, –109, –106, –102 and –96 in the ^{29}Si MAS NMR spectra were ascribed to Si(0Al), Si(1Al), Si(OH) and $Si(OH)_2$ species, respectively.

NH_3-TPD was used to evaluate the acidity of the nanosized ZSM-22 samples with different crystal sizes. As is shown in Fig. 7, all the samples exhibited two desorption peaks: a low-temperature peak at 480 K and a high-temperature peak at 713 K, corresponding to weak acid sites and strong acid sites, respectively. With increasing Si/Al ratio, there were slight shifts toward lower temperature, suggesting a decreased strength of the strong and weak acid sites caused by the reduction of Al atoms in the framework of ZSM-22. The results discussed above showed that the Si/Al ratio of the initial gel mixture has a significant effect on the physical and chemical properties of the N-ZSM-22 samples.

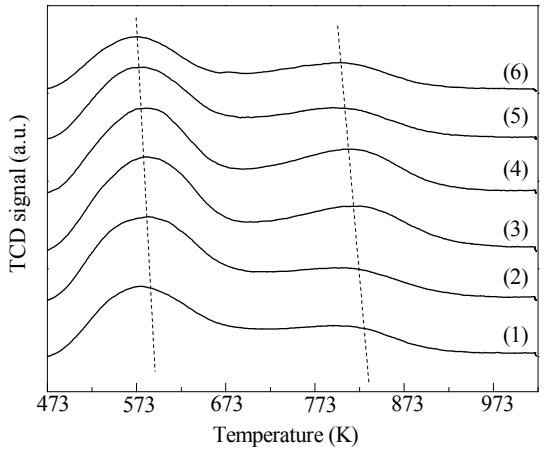

Fig. 7. NH_3-TPD profiles of N-ZSM-22 with varying Si/Al ratios: (1) 30; (2) 45; (3) 60; (4) 75; (5) 90. (6) M-ZSM-22 with Si/Al ratio of 90.

3.1.3. Effect of ethanol

Several techniques have been used to control the morphology and crystal size of zeolites. Beside the synthesis conditions such as rotation speed and composition of starting gel, organic solvents like alcohols and diols have also been reported as a promising alternative to control the morphology and crystal size of zeolites [37]. Here, ethanol was used in the synthesis mixture of the zeolite for the purpose of tuning the crystal morphology and crystal size of ZSM-22.

The XRD pattern of the obtained M-ZSM-22 sample is shown in Fig. 3(6). A phase-pure ZSM-22 was still obtained, suggesting that adding ethanol to the starting gel did not change the formation of the zeolite crystal phase. The morphologies and crystal sizes of the sample were characterized by SEM. The SEM image is shown in Fig. 4(e). Clearly, the sample consisted of

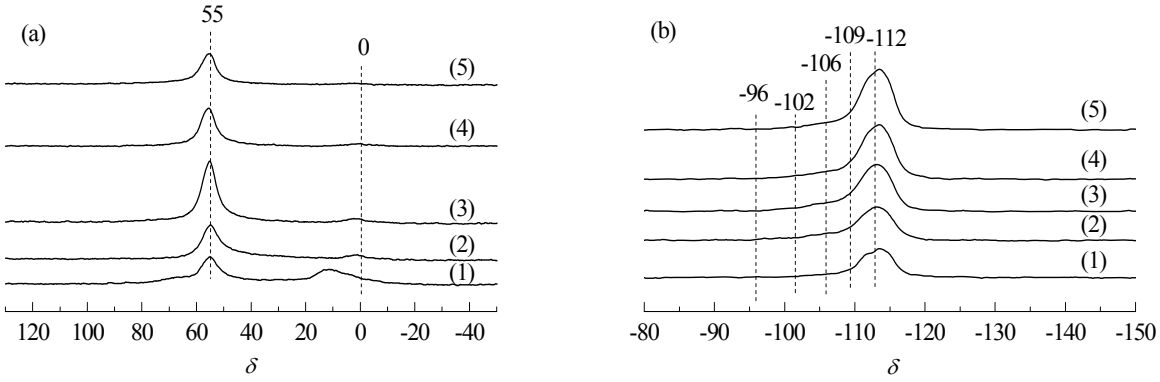

Fig. 6. ^{27}Al MAS NMR (a) and ^{29}Si MAS NMR (b) spectra of N-ZSM-22 samples with different Si/Al ratios: (1) 30; (2) 45; (3) 60; (4) 75; (5) 90.

needle-shaped crystals with crystal size of 7.2 μm. Compared to nanosized ZSM-22, the addition of ethanol effectively induced the elongation of ZSM-22 crystals to form bigger particles. The N_2 adsorption isotherm of M-ZSM-22 is shown in Fig. 5(6) and the textural properties of the sample are listed in Table 1. Compared to M-ZSM-22, the larger external surface area of N-ZSM-22 benefits a high surface activity. The acid property of M-ZSM-22 was also characterized by NH_3-TPD. The high-temperature and low-temperature desorption peaks were shifted down to lower temperatures for M-ZSM-22, indicating a decreased strength of the strong acid sites and weak acid sites with increasing Si/Al ratio.

3.2. Catalytic performance

Due to the unique one-dimensional pore system and small pore opening size, ZSM-22 has been reported to be useful in the conversion of methanol to olefins (MTO) [38,39]. The crystal size was reported to have important effects on the conversion of methanol for SAPO-34 and ZSM-5. However, there are few reports yet regarding the effect of ZSM-22 crystal size on the conversion of methanol. Here, the prepared nanosized and microsized ZSM-22 samples were tested in the conversion of methanol.

Fig. 8 presents the effects of zeolite crystal size on methanol conversion and product distribution with time on stream (TOS). As shown in Fig. 8(a), M-ZSM-22 with the larger crystal size deactivated faster than N-ZSM-22. The conversion of methanol declined with TOS due to coke formation on the acid sites located on the pore mouths and external surface [40]. In addition, the enhancement of reactant and product diffusion in the nanosized ZSM-22 also benefited a longer catalyst lifetime. Thus, the large external surface area and smaller crystal size effectively slowed down the deactivation of the catalyst as previously reported.

At the beginning of the reaction, methanol was completely converted to hydrocarbons over N-ZSM-22 and M-ZSM-22. Light olefins, which included ethylene, propylene and butylene, were the major products. The total selectivity to ethylene and propylene was almost the same for both N-ZSM-22 and M-ZSM-22. The selectivity to ethylene and aromatics over N-ZSM-22 was higher than that over M-ZSM-22. It was found that the initial low but detectable production of olefins over both zeolites was catalyzed by external and/or pore mouth acid sites by the hydrocarbon pool mechanism [40]. Therefore, the larger external surface area of N-ZSM-22 benefited a higher selectivity of ethylene and aromatics.

The effects of Si/Al ratio of the ZSM-22 zeolite on methanol conversion was also investigated (Fig. 8(a)). Considering the more extra-framework octahedral Al species in the N-ZSM-22 samples with Si/Al ratios of 30 and 45 (Fig. 6), the catalytic performance of N-ZSM-22 with Si/Al ratios of 60, 75 and 90 was investigated. As shown in Fig. 8(a), methanol was completely converted to hydrocarbons at the beginning of the reaction for all the nanosized ZSM-22 zeolite. It has been reported that with the decrease of Si/Al, the acid strength of the zeolite increased and the zeolite deactivated faster. However, N-ZSM-22 with Si/Al ratios of 90 deactivated faster than N-ZSM-22 with Si/Al ratios of 75 and 60. The probably reason was the larger crystal size of N-ZSM-22 with Si/Al ratio of 90, which is in accordance with the above results. The product distribution of N-ZSM-22 with different Si/Al ratios in the conversion of methanol are shown in Fig. 8(b). As shown, the selectivity of light olefins including ethylene and propylene increased with increasing of Si/Al ratio, while the selectivity of aromatics decreased. The results discussed above suggested that the higher Si/Al ratio facilitated the formation of light olefins and prevented the formation of aromatics.

4. Conclusions

Nanosized ZSM-22 with various Si/Al ratios was synthesized by a modified hydrothermal method using a relatively low rotation speed. The nano-crystal structure of ZSM-22 was confirmed by XRD and SEM. Through tuning the rotation speed and Si/Al ratio, nanosized ZSM-22 with crystal size in the range of 150–800 nm was synthesized. Ethanol as co-solvent used in the precursor gel induced the elongation of the ZSM-22 crystals to form bigger particles. The catalytic performance of the ZSM-22 zeolite samples was tested with the conversion of

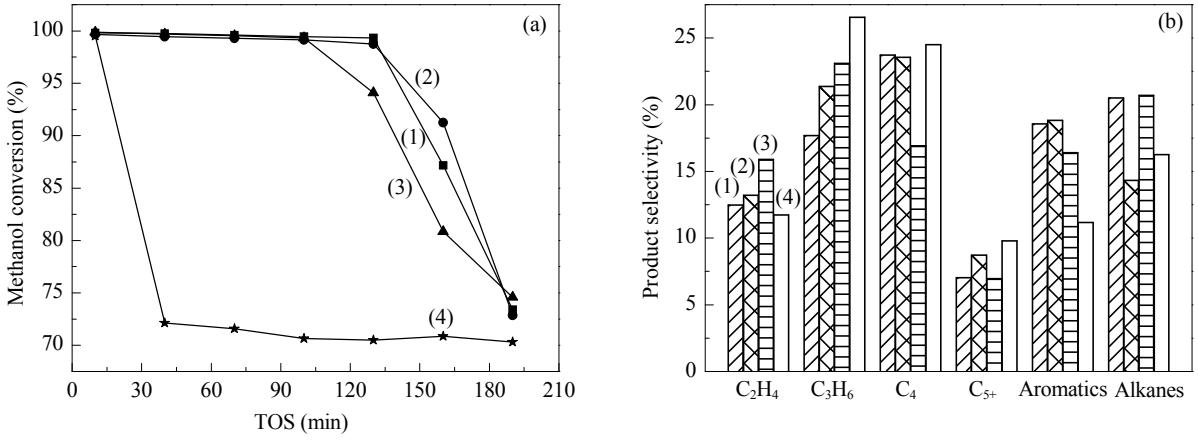

Fig. 8. (a) Methanol conversion as a function of time on stream (TOS) at 753 K with WHSV of 1.60 h^{-1} and (b) the product distribution at 10 min on N-ZSM-22 with Si/Al ratios of (1) 60, (2) 75, and (3) 90 and (4) M-ZSM-22 with Si/Al ratio of 90.

methanol. Compared to conventional ZSM-22, the nanosized ZSM-22 zeolite exhibited superior stability for the conversion of methanol. A higher external surface area and reduced particles size made this nanosized ZSM-22 zeolite attractive for catalytic applications.

References

[1] M. G. Clerici, *Top. Catal.*, **2000**, 13, 373–386.
[2] A. Corma, *J. Catal.*, **2003**, 216, 298–312.
[3] J. F. Denayer, A. R. Ocakoglu, W. Huybrechts, J. A. Martens, J. W. Thybaut, G. B. Marin, G. V. Baron, *Chem. Commun.*, **2003**, 1880–1881.
[4] C. Marcilly, *J. Catal.*, **2003**, 216, 47–62.
[5] S. Mintova, J. P. Gilson, V. Valtchev, *Nanoscale*, **2013**, 5, 6693–6703.
[6] S. Mintova, M. Jaber, V. Valtchev, *Chem. Soc. Rev.*, **2015**, 44, 7207–7233.
[7] A. G. Machoke, A. M. Beltran, A. Inayat, B. Winter, T. Weissenberger, N. Kruse, R. Guettel, E. Spiecker, W. Schwieger, *Adv. Mater.*, **2015**, 27, 1066–1070.
[8] K. Na, C. Jo, J. Kim, K. Cho, J. Jung, Y. Seo, R. J. Messinger, B. F. Chmelka, R. Ryoo, *Science*, **2011**, 333, 328–332.
[9] J. Gu, Z. Y. Zhang, P. Hu, L. P. Ding, N. H. Xue, L. M. Peng, X. F. Guo, M. Lin, W. P. Ding, *ACS Catal.*, **2015**, 5, 6893–6901.
[10] A. Ghorbanpour, A. Gumidyala, L. C. Grabow, S. P. Crossley, J. D. Rimer, *ACS Nano*, **2015**, 9, 4006–4016.
[11] C. Covarrubias, R. Quijada, R. Rojas, *Microporous Mesoporous Mater*, **2009**, 117, 118–125.
[12] V. Valtchev, L. Tosheva, *Chem. Rev.*, **2013**, 113, 6734–6760.
[13] L. Tosheva, V. P. Valtchev, *Chem. Mater.*, **2005**, 17, 2494–2513.
[14] R. Ravishankar, C. E. A. Kirschhock, P. P. Knops-Gerrits, E. J. P. Feijen, P. J. Grobet, P. Vanoppen, F. C. De Schryver, G. Miehe, H. Fuess, B. J. Schoeman, P. A. Jacobs, J. A. Martens, *J. Phys. Chem. B*, **1999**, 103, 4960–4964.
[15] C. Madsen, C. J. H. Jacobsen, *Chem. Commun.*, **1999**, 673–674.
[16] I. Schmidt, C. Madsen, C. J. H. Jacobsen, *Inorg. Chem.*, **2000**, 39, 2279–2283.
[17] J. A. Martens, W. Souverijns, W. Verrelst, R. Parton, G. F. Froment, P. A. Jacobs, *Angew. Chem. Int. Ed.*, **1995**, 34, 2528–2530.
[18] J. A. Martens, D. Verboekend, K. Thomas, G. Vanbutsele, J. P. Gilson, J. Perez-Ramirez, *ChemSusChem*, **2013**, 6, 421–425.
[19] G. Majano, A. Darwiche, S. Mintova, V. Valtchev, *Ind. Eng. Chem. Res.*, **2009**, 48, 7084–7091.
[20] Y. Y. Hu, C. Liu, Y. H. Zhang, N. Ren, Y. Tang, *Microporous Mesoporous Mater*, **2009**, 119, 306–314.
[21] J. H. Zhou, H. Jiang, J. Xu, J. Hu, H. L. Liu, Y. Hu, *J. Nanosci. Nanotechnol.*, **2013**, 13, 5736–5743.
[22] K. Moeller, B. Yilmaz, R. M. Jacubinas, U. Mueller, T. Bein, *J. Am. Chem. Soc.*, **2011**, 133, 5284–5295.
[23] A. A. Ismail, R. M. Mohamed, O. A. Fouad, I. A. Ibrahim, *Cryst. Res. Technol.*, **2006**, 41, 145–149.
[24] H. van Heyden, S. Mintova, T. Bein, *Chem. Mater.*, **2008**, 20, 2956–2963.
[25] O. Larlus, S. Mintova, T. Bein, *Microporous Mesoporous Mater.*, **2006**, 96, 405–412.
[26] G. T. Kokotailo, J. L. Schlenker, F. G. Dwyer, E. W. Valyocsik, *Zeolites*, **1985**, 5, 349–351.
[27] S. Parmar, K. K. Pant, M. John, K. Kumar, S. M. Pai, B. L. Newalkar, *Energy Fuels*, **2015**, 29, 1066–1075.
[28] M. A. Asensi, A. Corma, A. Martinez, M. Derewinski, J. Krysciak, S. S. Tamhankar, *Appl. Catal. A*, **1998**, 174, 163–175.
[29] R. Kumar, P. Ratnasamy, *J. Catal.*, **1989**, 116, 440–448.
[30] N. Kumar, L. E. Lindfors, R. Byggningsbacka, *Appl. Catal. A*, **1996**, 139, 189–199.
[31] D. Masih, T. Kobayashi, T. Baba, *Appl. Catal. A*, **2007**, 3303–3305.
[32] J. B. Wang, S. T. Xu, J. Z. Li, Y. C. Zhi, M. Z. Zhang, Y. L. He, Y. X. Wei, X. W. Guo, Z. M. Liu, *RSC Adv.*, **2015**, 5, 88928–88935.
[33] H. M. Wen, Y. Zhou, J. Y. Xie, Z. Y. Long, W. Zhang, J. Wang, *RSC Adv.*, **2014**, 4, 49647–49654.
[34] O. Muraza, A. Abdul-lateef, T. Tago, A. B. D. Nandiyanto, H. Konno,

Graphical Abstract

Chin. J. Catal., 2016, 37: 1381–1388 doi: 10.1016/S1872-2067(15)61099-3

Hydrothermal synthesis of nanosized ZSM-22 and their use in the catalytic conversion of methanol

Lei Chen, Peng Lu, Yangyang Yuan, Li Xu, Xiaomin Zhang*, Lei Xu*
Dalian Institute of Chemical Physics, Chinese Academy of Sciences; University of Chinese Academy of Sciences

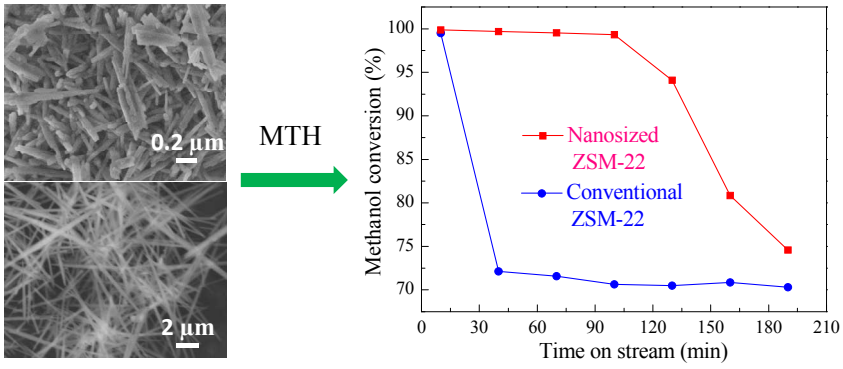

Different crystal length ZSM-22 zeolite samples were prepared using a modified hydrothermal synthesis method. Nanosized ZSM-22 showed better catalytic stability in the conversion of methanol.

Y. Nakasaka, Z. H. Yamani, T. Masuda, *Microporous Mesoporous Mater.*, **2015**, 206, 136–143.
[35] L. Shirazi, E. Jamshidi, M. R. Ghasemi, *Cryst. Res. Technol.*, **2008**, 12, 1300–1306.
[36] Y. Liu, Z. D. Wang, Y. Ling, X. B. Li, Y. M. Liu, P. Wu, *Chin. J. Catal.*, **2009**, 30, 525–530.
[37] A. K. Jamil, O. Muraza, A. M. Al-Amer, *J. Ind. Eng. Chem.*, **2015**, 29, 112–119.
[38] J. Z. Li, Y. X. Wei, Y. Qi, P. Tian, B. Li, Y. L. He, F. X. Chang, X. D. Sun, Z. M. Liu, *Catal. Today*, **2011**, 164, 288–292.
[39] S. Teketel, U. Olsbye, K. P. Lillerud, P. Beato, S. Svelle, *Appl. Catal. A*, **2015**, 494, 68–76.
[40] F. F. Wei, Z. M. Cui, X. J. Meng, C. Y. Cao, F. S. Xiao, W. G. Song, *ACS Catal.*, **2014**, 4, 529–534.